Modeling of a 3D plasma thermal spraying and the effect of the particle injection angle

D. Khelfi[1*], A. Abdellah El-Hadj[2] and N. Aït-Messaoudène[3]

[1] Centre de Recherche Nucléaire de Birine, COMENA, Algérie
[2] Laboratoire LMP2M, Université de Médéa, Algérie
[3] Laboratoire des Applications Energétiques de l'Hydrogène, Université de Blida, Algérie

Résumé - *Une comparaison a été faite entre deux modèles de turbulence k - ε et RNG d'un jet de plasma d'argon/hydrogène déchargé dans l'air. Le jet de plasma d'argon déchargé dans l'air est simulé par les modèles k - ε et RNG pour une configuration 3D. Le comportement des particules a été modélisé à l'aide des trajectoires de particules solides. Les calculs sont effectués avec le code CFD Fluent. Tout d'abord, on a fait une validation pour la projection des particules de Ni et de ZrO_2. Cette partie de l'étude montre que les paramètres des particules sont mieux prédits avec le modèle RNG. Enfin, nous avons constaté que l'angle d'injection des particules a un effet important sur le chauffage et l'accélération des particules.*

Abstract - *A comparison is made between two turbulence models for an argon/hydrogen plasma discharged into air atmosphere. Three dimensional plasma jet flow is predicted with the standard k - ε model and the RNG model of turbulence. Particles behaviour has been modelled by using stochastic particles trajectories. Computations are performed with the Fluent CFD code. First, a validation is made for spray parameters of Ni and ZrO_2 particles. This part of the study shows that the particle parameters are better predicted with the RNG model. Finally, we have found that the particle injection angle has an important effect on particle heating and acceleration.*

Keywords: Plasma spraying - k - ε - RNG - Injection angle.

1. INTRODUCTION

Thermal plasmas have found extensive industrials applications in the area of materials processing, such as plasma spraying, cutting, welding, ultra-fine particle synthesis, etc. [1]. Plasma spraying consists of injecting solid particles into a high temperature, high velocity gas jet, in which the jet acts as a transport medium for heating and accelerating the spraying particles.

Acceleration and heating of particles are crucial in thermal spraying to both process efficiency and coating quality. For a given process, the particles need to achieve a specific range of thermal and kinetic energy. In many cases, the parameters that affect the heating and motion of particles are interrelated and interaction effects are complex. In order to better understand the thermal spray process, great efforts have been performed in the last years in the area of theoretical modeling.

Research efforts have been devoted to plasma jet characteristics and the behavior of injected particles in the plasma jet. Yet, the physics of plasma thermal spraying remains little controlled. One of the major difficulties is the presence of turbulence which complicates the modeling of thermal plasma, preventing a full understanding of the plasma-particle interaction phenomena. The complement brought by simulation to

* Khelfi_djillali@hotmail.com _ lmp2m_cum@yahoo.fr _ naitmessaoudene@yahoo.com

experimental measurements is essential because measurements are often difficult to realize considering the range of temperatures concerned.

Most of the simulations have been conducted in a 2D computational domain. Two-dimensional models suppose an axial symmetry [2-5]. 2D modeling can significantly simplify the numerical efforts. However, it cannot simulate any three-dimensional (3D) process occurring in thermal plasma systems. But 3D modeling of thermal plasma systems is still a challenging problem, as demonstrated by some recent publications [6-10]. Most of them were performed using commercial CFD software. Since the 1980s, both the methodology in computational fluid dynamics (CFD) and computing capacities have greatly improved.

As a result, CFD has been applied to plasma spray research since early 1990's and offers a great potential for process optimization. Several researchers have used a CFD code to simulate plasma spraying processes. For example, D.T. Gawne *et al.* [7] study the effects of radial injection of a water jet into swirl and no swirl plasma jets. The authors use the Star-CD CFD code to solve the problem. K. Ramachadran *et al.* [8], study the effects of radial injection of water jet into swirl and non-swirl plasma jets.

The authors use the Phoenics CFD code. Y.Y. Zhao *et al.* [11] developed a numerical model to calculate spatial distributions of plasma gas temperature, enthalpy, velocity and fractions of dissociated and ionized species in a vacuum plasma spraying. The authors use the Fluent CFD code. Ahmed *et al.* [12] studied the behavior of ceramic particles in Ar-H_2 plasma jet using a 3D model coupled with the commercial computational code Fluent.

The $k-\varepsilon$ turbulence model is exclusively used in plasma spraying modeling. The standard $k-\varepsilon$ model falls within the simplest two-equation turbulence models. A popular alternative model is the RNG (ReNormalized Group) turbulence model. The RNG turbulence model [13] was derived using a rigorous statistical technique (renormalized group theory).

In addition to high Reynolds number effects, the RNG model also takes into account low Reynolds number effects and it can even predict some laminar behavior. The RNG model improves predictions for high streamline curvature and strain rate, transitional flows, and wall heat and mass transfer. In this study, we begin performing a comparison between two models of turbulence, the $k-\varepsilon$ model and RNG model for an Argon plasma jet flow discharged into air environment.

Next, we investigate the comparison between the two models of turbulence for modeling the particle behavior during Ar/H_2 plasma thermal spraying. Finally, we study the effects of injection direction or injection angle on particle behavior during plasma thermal spraying.

2. MATHEMATICAL MODEL

The plasma torch, the injection port, and the substrate are schematically shown in figure 1.

2.1 Plasma jet

The gaseous species are supposed to behave as ideal gases at atmospheric pressure. The system is in steady state, with time-averaged turbulent fluctuations taken into account. The plasma components are in local thermodynamic equilibrium. In addition,

the plasma is modeled as a turbulent free jet composed of a high temperature mixture of Ar-H_2 issuing into ambient air.

The transport properties for gases (plasma (Ar and H_2) and air) are calculated from data reported in Boulous *et al.* [14]. The transport properties are calculated based on the Chapman-Enskog theory. Mixture transport properties are calculated with the Wilke's formula [14]. Because of their anticipated small effect on sprayed particles and the expense of including them in a fully elliptic three-dimensional simulation, chemical reactions within the plasma are not modeled here.

It is estimated that the reactions would contribute to less than 10 percent of the particle heating. It is noted that a higher level of uncertainty is associated with values of transport properties [14]. The effect of neglecting chemical reactions for plasma jet simulation has been adopted in a number of recent works [7, 8, 12].

The equations to be solved for the gases are conservation of mass, momentum, enthalpy, species (Ar, H_2 and air), and turbulence kinetic energy as well as its dissipation as presented in [9]. Two models of turbulence are used in the study, the $k-\varepsilon$ model and the RNG model [13].

A general-purpose CFD code, Fluent, is used in this study. Fluent uses FVM (Finite Volume Method) [15] for predicting the fluid dynamics of the plasma jet and the ambient air. The transport equations are set in integral form:

$$\underbrace{\frac{\partial}{\partial t}\int_V \rho.\phi.dV}_{\text{Unsteady}} + \underbrace{\int_A \rho.\phi.V.dA}_{\text{Convection}} = \underbrace{\int_A \Gamma.\nabla\phi.dA}_{\text{Diffusion}} + \underbrace{\int_V S_\phi.dV}_{\text{Generation}} \quad (1)$$

Where ϕ is a variable that is used to describe a general transportable quantity, and S_ϕ is the source term [16]. **Table 1**, gives a subset of the variables that are solved. Field variables (stored at cell centers) must be interpolated to the faces of the control volumes in the FVM according to:

$$\frac{(\rho\phi)^{t+\Delta t}-(\rho\phi)^t}{\Delta t}.\Delta V + \sum_{\text{Faces}} \rho_F.\phi_F.V_F.A_F = \sum \Gamma_F(\nabla\phi)_{\perp,F}.A_F + S_\phi.\Delta V \quad (2)$$

Table 1: Corresponding ϕ for transport equations

Equation	Variable for ϕ
Continuity	1
Momentum (x, y, z)	Velocity (u, v, w)
Energy	Enthalpy (h)
Turbulent Kinetic energy	K
Turbulent dissipation rate	ε
Species transport	Mass fraction of species (Y_i)

The transport equation for ϕ is presented in a simple form: $a_P.\phi_P + \sum a_{nb}.\phi_{nb} = b_b$. The solution converges, if the residue $R = \sum_{\text{cells}} |R_P|$ is small enough for all equations, where $R_P = a_P.\phi_P + \sum a_{nb}.\phi_{nb} - b_b$.

The standard Fluent interface cannot be programmed to anticipate every user's needs. The use of UDFs (User Defined Function), however, enables the user to

customize the code to fit particular modeling needs. UDFs can be used for a variety of applications [16]. Thermophysical properties and inlet velocity and temperature are set by UDF functions.

For the two turbulence models ($k-\varepsilon$ model and RNG model), the turbulent kinetic energy equation is:

$$\frac{\partial(\rho u k)}{\partial x}+\frac{\partial(\rho v k)}{\partial y}+\frac{\partial(\rho w k)}{\partial z}=\frac{\partial}{\partial x}\left(\frac{\mu_t}{\sigma_k}\frac{\partial k}{\partial x}\right)+\frac{\partial}{\partial y}\left(\frac{\mu_t}{\sigma_k}\frac{\partial k}{\partial y}\right)+\frac{\partial}{\partial z}\left(\frac{\mu_t}{\sigma_k}\frac{\partial k}{\partial z}\right)+\mu_t\Phi-\rho\varepsilon \qquad (3)$$

The dissipation rate equation is:

$$\frac{\partial(\rho u\varepsilon)}{\partial x}+\frac{\partial(\rho v\varepsilon)}{\partial y}+\frac{\partial(\rho w\varepsilon)}{\partial z}=\frac{\partial}{\partial x}\left(\frac{\mu_t}{\sigma_\varepsilon}\frac{\partial \varepsilon}{\partial x}\right)+\frac{\partial}{\partial y}\left(\frac{\mu_t}{\sigma_\varepsilon}\frac{\partial \varepsilon}{\partial y}\right)+\frac{\partial}{\partial z}\left(\frac{\mu_t}{\sigma_\varepsilon}\frac{\partial \varepsilon}{\partial z}\right)+C_{1\varepsilon}\mu_t\frac{\varepsilon}{k}\Phi-C_2\rho\frac{\varepsilon^2}{k} \qquad (4)$$

Where ϕ, the viscous dissipation term, in tensor notation is given by:

$$\Phi = \mu\left(\frac{\partial u_i}{\partial x_k}+\frac{\partial u_k}{\partial x_i}\right)\frac{\partial u_i}{\partial x_k} \qquad (5)$$

Default values for various constants in the standard model are given in **Table 2** [14].

Table 2: Standard model coefficients

$C_{1\varepsilon}$	C_2	C_μ	σ_k	σ_ε
1.44	1.92	0.09	1.0	1.3

In the RNG model [13] a constant C_μ is used. The value is specified with a separate command than the one used to specify the C_μ in the standard model. The same is true of the constant C_2. As shown in the above table, the diffusion multipliers have different values than the default model, and these parameters also have their own commands for the RNG model. Quantities in equations (3) et (4) not specified in **Table 2** are covered by **Table 3**.

Table 3: RNG model coefficients

C_2	C_μ	σ_k	σ_ε	β	η_∞
1.68	0.085	072	4.38	0.12	4.38

In the RNG model, the constant $C_{1\varepsilon}$ in dissipation equation is replaced by a function of one the invariants:

$$C_{1\varepsilon} = 1.42-\frac{\eta\left(1-\frac{\eta}{\eta_\infty}\right)}{1+\beta\eta^3} \qquad (6)$$

The invariant η is given by:

$$\eta = \frac{k}{\varepsilon}\sqrt{2S_{ij}.S_{ij}} \qquad (7)$$

Where S_{ij} is the symmetric deformation tensor equal to $\frac{1}{2}\left(u_{i,j}+u_{j,i}\right)$.

The solution of the turbulence equations is used to calculate the effective viscosity:

$$\mu_e = \mu + C_\mu \rho \frac{k^2}{\varepsilon} \tag{8}$$

2.2 Computational domain and boundary conditions

The boundary conditions are based on the physical configuration described in Fig. 1.

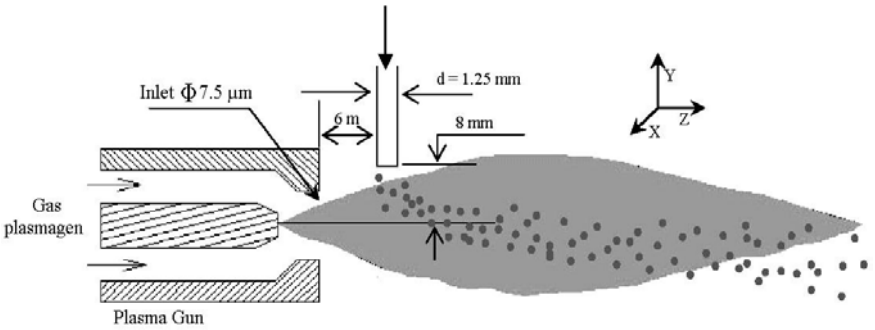

Fig. 1: Illustration of the computational domain

The computational grid is polar cylindrical, with dimensions of 50 mm, 180 mm and 2π radians in the radial, axial, and azimuthal directions. The mesh is more refined near the axis in the radial direction as well as near the jet exit in the axial direction. It is uniform in the angular direction. An analysis of different mesh dimensions reveals that 60 nodes in X direction, 50 in r direction, and 34 in θ direction are sufficient.

The velocity and temperature at the nozzle exit are prescribed and given by [18]:

$$v = 0,\ w = 0 \text{ and } u = u_m \cdot \left(1 - \left(\frac{r}{R}\right)^n\right) \tag{9}$$

$$T = (T_m - T_a) \cdot \left(1 - \left(\frac{r}{R}\right)^m\right) + T_a \tag{10}$$

Where u_m and T_m are the maximum velocity and temperature at the plasma jet centerline and R the inner radius of the nozzle. T_a is the nozzle wall temperature which is taken as 300 K. The exponents values in the equations above are m = 4.5 and n = 2 [18]. The turbulence intensity $I = \frac{u'}{u}$, u' being RMS of the fluctuating component) is specified along with the length scale (l) set to the torch exit diameter (hence at the torch exit $k = \frac{3}{2}u'^2$, $\varepsilon = \frac{C_\mu^{3/4} k^{3/2}}{l}$).

The effect of DC arc fluctuations, which are originally driven by random arc initiation and extinction between the cathode and the anode, is not a true turbulence phenomenon. However, because of the lack of understanding of the detailed arc physics, this fluctuation is accounted for by specifying a high level of turbulence at the jet exit, with $I = 20$ percent [19]. The two equations turbulence models will not predict correct

near-wall behavior if integrated all the way down to the wall. A special near-wall treatment is required. We use the standard wall functions for the velocity and temperature fields.

2.3 Particles-plasma interactions

Lagrangian equations of motion and heat balance are used to simulate the particle behavior in the plasma jet. Dilute sprays assumption is considered here, where cooling and redirection of plasma gases by the particles is neglected. Thus, one way coupling is used for the discrete phase [16]. The velocity of a particle can be calculated according to the force balance on the particle [16]:

$$\frac{d\vec{v}_P}{dt} = F_D\left(\vec{v} - \vec{v}_P\right) + F_{th} \tag{11}$$

where $\vec{v}_P$ and $\vec{v}$ are the particle and gas velocities respectively, and F_D is the drag force per unit particle mass, which is given by:

$$F_D = \frac{18\mu}{\rho_P . d_P^2}\frac{C_D\,Re}{24} \tag{12}$$

where ρ_P is the particle density, d_P is the particle diameter, C_D is the drag coefficient and Re is the relative Reynolds number defined as: $Re = \dfrac{\rho . d_P . \left|\vec{v}_P - \vec{v}\right|}{\mu}$.

The drag coefficient C_D is a function of the relative Reynolds number:

$$C_D = a_1 + \frac{a_2}{Re} + \frac{a_3}{Re^2} \tag{13}$$

where a_1, a_2 and a_3 are constants given by Morsi and Alexander [16].

Small particles suspended in a gas that has a temperature gradient experience a force in the direction opposite to that of the gradient. This phenomenon is known as thermophoresis. Fluent can optionally include a thermophoresis force on particles in the additional force term intended for this purpose. The expression of the thermophoresis force suggested by Tablot [16] is given by:

$$F_{th} = -\frac{-6\pi . d_P . \mu^2 . C_S . \left(K' + C_t\,kn\right)}{\rho\left(1 + 3C_m\,kn\right)\left(1 + 2K' + 2C_t\,kn\right)}\frac{1}{m_p T}\frac{\partial T}{\partial x} \tag{14}$$

C_S, C_m, C_t are model constants [16]. kn is the Knudsen number. $K' = \dfrac{k_p}{k_g}$, where k_p is the particle thermal conductivity and k_g the gas thermal conductivity.

In the present work, a particle stochastic trajectory model is used. The particles are assumed to be deflected by eddies when they cross them. The time of particle interaction with the randomly sampled field (eddies) is assumed to be the minimum of the eddy lifetime and transit time required for the particle to cross the eddy. The eddy lifetime and particle transit time are given as:

$$\Delta t_e = \frac{l_e}{\left|\vec{v}'\right|} \tag{15}$$

$$\Delta t_\gamma = \frac{l_e}{\left|\vec{v'} - \overrightarrow{v_P}\right|} \tag{16}$$

where the eddy size is:

$$l_e = \frac{C_\mu^{3/4} k^{3/2}}{\varepsilon} \tag{17}$$

Assuming that the particle is heated by convective and radiation heat transfer only, the temperature is uniform throughout the particle and there are no phase transformations in the particle. The particle temperature can be calculated from [16]:

$$m_P C_P \frac{dT_P}{dt} = \eta . A\left(T - T_P\right) + \varepsilon_P . A . \sigma\left(\theta_R^4 - T_P^4\right) \tag{18}$$

where m_P is the mass of the particle, C_P is the specific heat of the particle, T_P is the particle temperature, A is the surface area of the particle, η is the convective heat coefficient, θ_R is the radiation temperature, ε_P is the particle emisivity, σ is the Stefan Boltzman constant ($5.67\ 10^{-8}$ W/m^{2}K^4) and T is the local gas temperature.

The heat transfer coefficient is evaluated using the Ranz-Marshall correlation [16]:

$$\eta = \frac{k_P \left(2.0 + 0.6\ Re^{1/2} . Pr^{1/3}\right)}{d_P} \tag{19}$$

Some factors are not included in the discrete phase model. Ait-Messaoudene *et al.* [20] presents a full particles model used in thermal spraying.

3. RESULTS AND DISCUSSION

3.1 Particles behavior

Results of previous model of particles (also using $k-\varepsilon$) and measurements [19] are compared with the present computations. The system used is Metco-9MB plasma spray torch. Operating conditions are: a torch current and voltage of 500 A and 70 V respectively. The gas composition is 40 slm of Ar and 12slm of H_2. The nozzle exit diameter is 7.5 mm. The particles to be injected have an initial temperature of 300 K.

Fig. 2-a shows the particle velocity for three theoretical models and the experimental data. For the sake of comparison, a group of 56 – 71 μm diameter of zirconium particles is used. The initial transverse inward velocity for zirconium particles is taken 14.5 m/s. For the velocity, results show that the RNG model is in better agreement with experimental measurements than the $k-\varepsilon$ model. In addition, Fig. 2-b shows a comparison of particles thermal history.

The RNG model still gives better results. For example, at 105 mm from the nozzle exit, the RNG model yields a velocity which is 23 % lower than experimental data. At the same position, the $k-\varepsilon$ model gives a result 45 % lower than experimental data. For the temperature at the same position, the differences compared to experimental data are 29 % and 99 % for the RNG and the $k-\varepsilon$ model respectively.

The same comparison for a group of nickel particles of 60 - 70 μm diameter is presented in figure 3. The initial transverse inward velocity for nickel particles is taken 9.8 m/s. In this figure, we can still see the advantage of the RNG model compared to the $k-\varepsilon$ model. For example, at 85 mm from the nozzle exit, the RNG model gives a

lower velocity compared with experimental data by approximately 70 %. At the same position, the $k-\varepsilon$ model underestimates the velocity by 30 %. For the temperature at the same position, the differences compared with experimental data are 11 % and 36 % for the RNG model and the $k-\varepsilon$ model respectively.

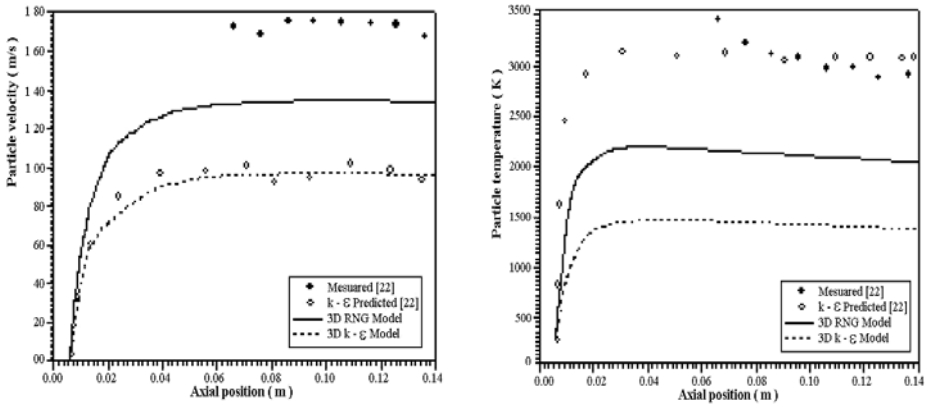

(a) (b)

Fig. 2: ZrO_2 Particle (a) velocity and (b) temperature along the axial distance in an Ar–H_2 Plasma jet

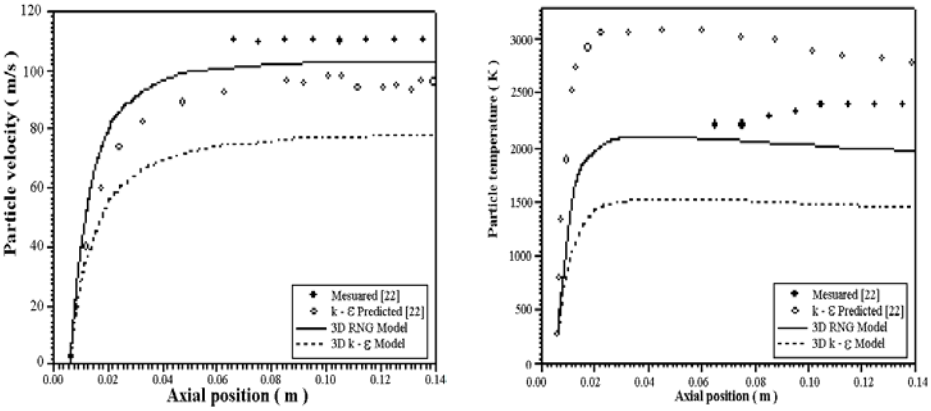

(a) (b)

Fig. 3: Nickel Particle (a) velocity and (b) temperature along the axial distance in an Ar–H_2 plasma jet

3.2 Effect of particle Injection angle

The last plasma system is used in this case. Here the injector angle with respect to the jet centerline is changed. A single particle of ZrO_2 is numerically injected into the plasma jet. Three particle sizes (30 μm, 50 μm and 70 μm) are used. In this part of the study, the effect of particle injection direction is investigated. We use three types of injection angles, vertical position, 45° upstream inclined injection and 45° downstream

inclined injection. The particle injection velocity is 14.5 m/s in magnitude for all cases. Fig. 4 illustrates these three injection possibilities.

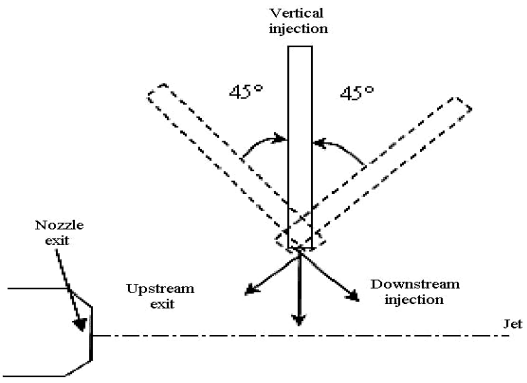

Fig. 4: Different particles injection configurations

Fig. 5 shows the velocity evolution along the jet axis. From this figure, we can see that upstream inclined injection increases the particle velocity as it moves upstream. It should be noted that at the injection position, upstream injection confers a lower initial axial velocity since particles are injected counter flow. By contrast, downstream injection leads a lower particle velocity.

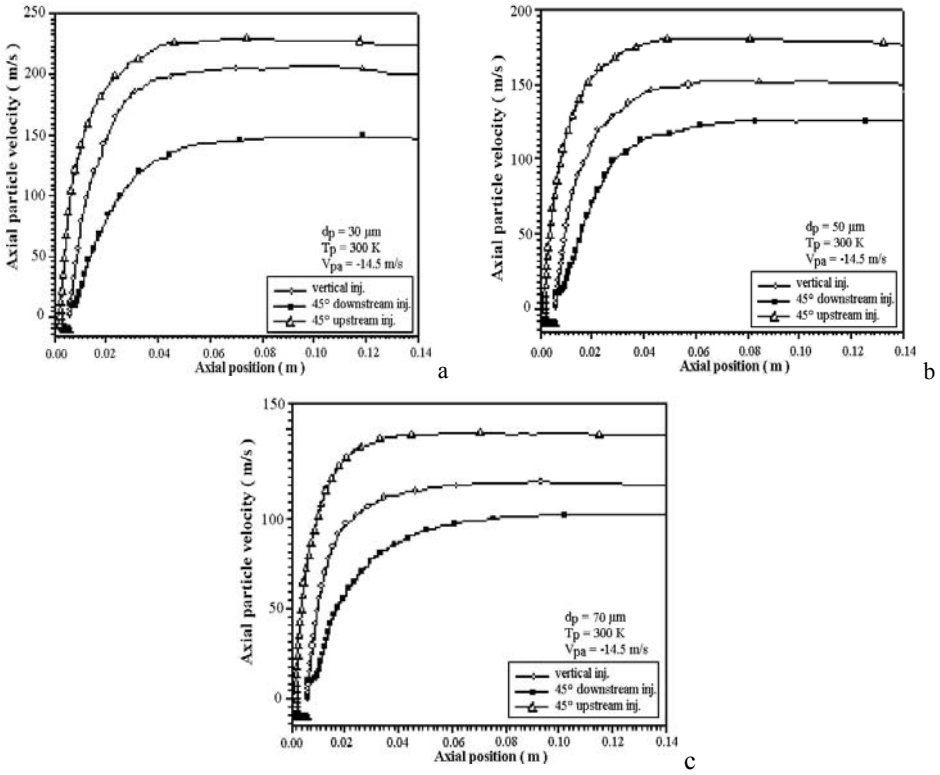

Fig. 5: Particle velocity along axial position for three injector directions

The temperature histories are illustrated in Fig. 6. In this case also, upstream injection gives higher values of temperature than the others. This is due to the fact that when particles are injected toward the nozzle exit region, encounter a higher energy and momentum regions of the plasma jet. This leads to a higher acceleration and heating of the particles. This seems an interesting result for real process applications and should be investigated experimentally.

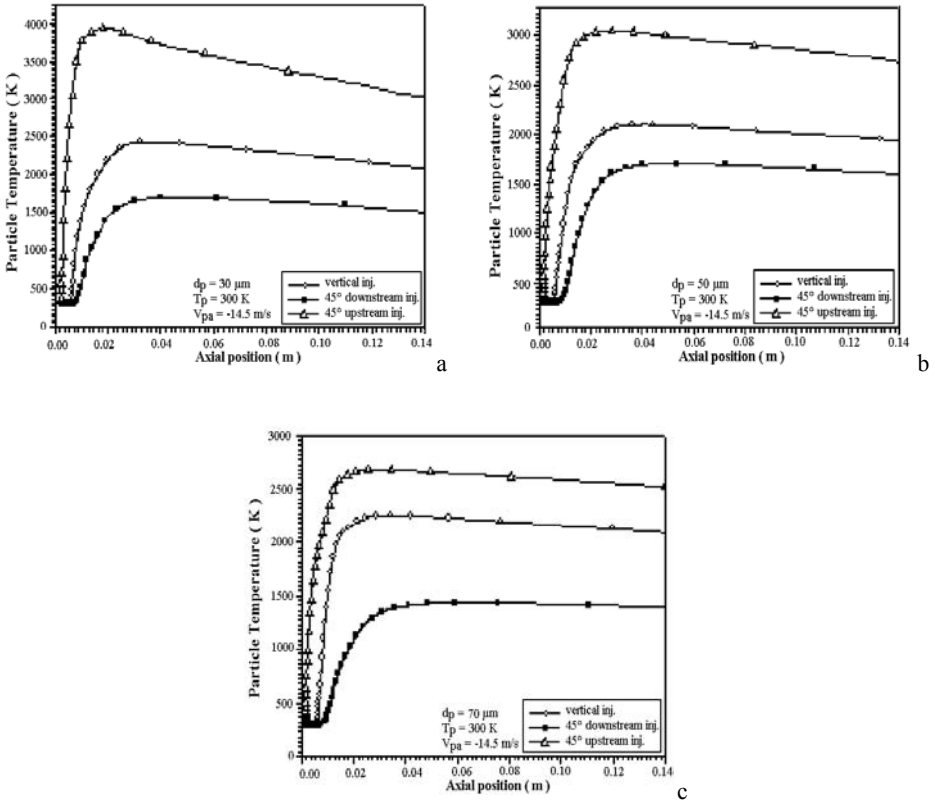

Fig. 6: Particle temperature along axial position for three injection directions

4. CONCLUSION

The main contribution of this study is the comparison of two turbulence models, $k-\varepsilon$ and RNG for the simulation a three dimensional plasma thermal spraying jet configurations.

In a first step, a comparison is made for the gases flow alone. The computations show that the RNG model is in better agreement with experimental data. Secondly, the motion and heating of particles in the jet during plasma spraying is simulated for nickel and ZrO_2 powders.

In this case again, the RNG model yields more realistic results compared to the $k-\varepsilon$ model. Therefore, although there is a little supplement in computation time with the RNG model, it should be preferred in plasma thermal spraying simulation studies.

Finally, the effect of the injection angle of the particles is investigated. For the same particle injection velocity magnitude, it is found upstream inclined injection leads to higher levels of heating and acceleration of the particles. This suggests a very simple process configuration change for enhancing coating quality. It should be interesting to confirm this result experimentally.

NOMENCLATURE

a_E, a_W, a_P, b : Constants of finite volumes mthod

a_1, a_2, a_3 : Constants

C_D : Coefficient of drag

C_p : Specific heat

C_μ, $C_{\varepsilon 1}$, $C_{\varepsilon 2}$, $C_{\varepsilon 3}$, β, σ_k et σ_ε : Constants of RNG and $k-\varepsilon$ model

D : Coefficient of diffusion

d : Diameter of the torch

d_p : Diameter of particle

F_d : Drag force

F_{th} : Thermal force

h : Enthalpie

I : Intensity of turbulence

K :Turbulent kinetic energy

K' : Ration of conductivities

l : Scale length

l_e : Dimension of the swirl

R : Inner radius of the nozzle

Re : Reynolds number

S_ϕ : Source term

T : Temperature

T_m : Maximum temperature at the plasma jet centreline

u_m : Maximum velocity at the plasma jet centerline

V : Velocity

u, ν, w : Constants of velocity

Y_i : Species

ε : Turbulent dissipation rate

η : Invariant

Γ : Coefficient of diffusion

ρ : Density

σ : Stefan-Bolzman constant

ϕ : Variable that is used to describe a general transportable quantity

Φ: Viscous dissipation term

Δt_e :Life time for the particle

RR : Residue

REFERENCES

[1] W. Smith and R.D. Fast, Welding Journal, Vol. 43, 1994.

[2] N. Elkaddah, J. Mckelliget and J. Szekely, Metallurgical Transactions B15B, Vol. 59, 1984.

[3]Y.C. Lee and E. Pfender, Plasma Chem., Plasma Process., Vol. 7, N°1, p. 1, 1987.

[4] P.C. Huang, T. Heberlein and E. Pfender, Surface and Coatings Technology, Vol. 73, p. 142, 1995.

[5] J. Park, J. Heberlein *et al.*, Plasma Chem., Plasma Process, Vol. 28, p. 213, 2008.

[6] Xi. Chen and H. Li, Surface and Coatings Technology, Vol. 171, p. 124, 2003.

[7] D.T. Gawne, T. Zhang and B. Liu, Surface and Coatings Technology, Vol. 153, p. 147, 2002.

[8] K. Ramachadran, N. Kikukawa and H. Nishiyama, Thin Solid Films, Vol. 435, p. 298, 2003.

[9] Juan Pablo Trelles, E. Pfender, *et al*., Plasma Chem. Plasma Process., Vol. 26, p. 557, 2006.

[10] E. Meillot, D. Guenadou, *et al.*, Plasma Chem Plasma Process, Vol. 28, p. 69, 2008.

[11] Y.Y. Zhao, P.S. Grant and B. Cantor, Modeling Simul. Mater Sci. Eng., Vol. 8, p. 514, 2000.

[12] I. Ahmed and T.L. Bergman, Transaction of ASME, Vol. 123, p. 188, 2001.

[13] V. Yakhot and S.A. Orszag, '*Renormalized Group Analysis of Turbulence: I-Basic theory*', J. Sci. Comput., Vol. 1, p. 3, 1986.

[14] M.I. Boulos, P. Fauchais and E. Pfender, '*Thermal Plasmas: Fundamentals and Applications*', Vol. 1, Plenum press, New York, 1994.

[15] S.V. Patankar, '*Numerical Heat Transfer and Fluid Flow*', Hemisphere Publ. corp., McGraw-Hill, 1980.

[16] Fluent Inc., Fluent V6 Manual, Lebanon, NH, USA, 1998.

[17] B.E. Launder and D.B. Spalding, '*The Numerical Computations of Turbulent Flows*', Computer Methods in Applied Mechanics and Engineering, Vol. 3, p. 269, 1974.

[18] C.H. Chang and J.D. Ramshaw, Plasma Chem. Plasma Process., Vol. 16, N°1, p. 5S, 1993.

[19] M.P. Planche, J.F. Coudert and P. Fauchais, Plasma Chem. Plasma Process., Vol. 18, p. 263, 1998.

[20] N. Ait-Messaoudene and A. Abdellah El-Hadj, Surface and Coating Technology, Vol. 106, p. 140, 1998.

[21] J.W. Mckelliget, G. Trapaga, E. Gutierrez-Miravete, M. Cyberlski, in: C. Coddet (Ed.), Proceedings of the 15th International Thermal Spray Conference, Nice, France, May 25-29, p. 335, 1998.

[22] Y.P. Wan, V. Gupta, Q. Deng, S. Sampath, V. Prasard, R. Williamson and J.R. Fincke, Journal of Thermal Spray Technology, Vol. 10, N°2, p. 383, 2001.